Article

Comparative Study on 3D Printed Ti6Al4V Scaffolds with Surface Modifications Using Hydrothermal Treatment and Microarc Oxidation to Enhance Osteogenic Activity

Leizhen Huang,[||] Bianyun Cai,[||] Yong Huang, Jingcheng Wang, Ce Zhu, Kun Shi, Yueming Song, Ganjun Feng,* Limin Liu,* and Li Zhang*

Read Online

ACCESS | Metrics & More | Article Recommendations
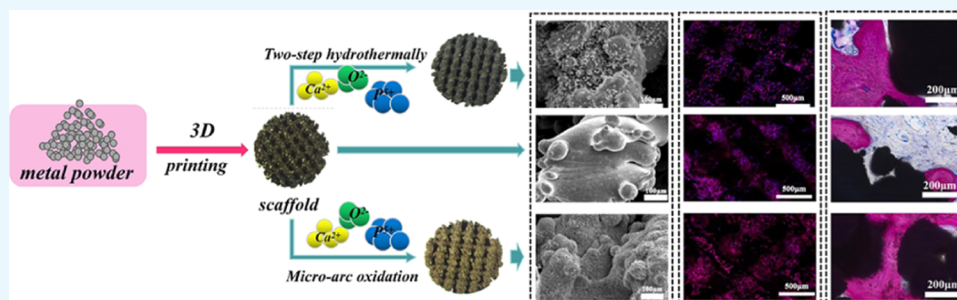
ABSTRACT: Titanium (Ti) and its alloys have been widely used in clinics as preferred materials for bone tissue repair and replacement. However, the lack of biological activity of Ti limits its clinical applications. Surface modification of Ti with bioactive elements has always been a research hotspot. In this study, to promote the osseointegration of Ti6Al4V (Ti64) implants, calcium (Ca), oxygen (O), and phosphorus (P) codoped multifunctional micro–nanohybrid coatings were prepared on a three-dimensional (3D) printed porous Ti64 surface by microarc oxidation (MAO) and a hydrothermal method (HT). The surface morphologies, chemical compositions, and surface/cell interactions of the obtained coatings were studied. *In vitro* experiments indicated that all hybrid coating-modified Ti64 implants could enhance protein adsorption and MC3T3 osteoblasts' activity, adhesion, and differentiation ability. *In vivo* experiments showed that the hybrid coating promoted early osseointegration. By comparison, microarc oxidation-treated Ti64 (M-Ti) has the best biological activity and the strongest ability of osseointegration. It provides important theoretical significance and potential application prospects for improving the biological activity of Ti implants.

1. INTRODUCTION

Titanium (Ti) and its alloys are the most widely used biomaterials in orthopedics[1] and have exerted their unique advantages, especially in load-bearing bone (*e.g.*, hip joint) repair or replacement, due to the dominant merits including superior mechanical strength, good biocompatibility, corrosion resistance, etc.[2] However, the lack of bioactivity as well as the much higher elastic modulus than human bone often affects the bone–implant interface, leading to inadequate initial osseointegration and surgical failure.[3] So far, a variety of surface treatments have been used to improve the bioactivity of Ti implants, some of which have displayed enhanced osseointegration and been applied clinically.[4,5] Even so, the failure cases (loosens, shifts, and falls off) caused by the stress shielding effect due to the high modulus of Ti implants are still common in clinics.[6]

To effectively solve the stress shielding effect, the pore structure optimization design of porous Ti is of great significance for the mechanical properties and biological

functions of customized materials. The three-dimensional (3D) printing technique is one of the most precise methods for preparing porous Ti alloy scaffolds according to patient-specific requirements.[7] In addition to bone ingrowth, another key to the strength of osseointegration is the stability of the bone/implant interface. It is reported that the surface morphology and chemical composition of porous scaffolds are the key factors affecting the stability of the bone/implant interface.[8,9] Although the 3D printing technique can well control the pore structure, the surface performances are beyond its control, so surface modification is still indispensable.

As known, human bone trabeculae are mainly composed of calcium (Ca) and phosphorus (P) and have a micro/nano multistage structure.[10] Compared with the smooth surface, on the one hand, the micro/nano multistage structure can increase the friction between the implant and the surrounding host bone, effectively avoid the micromovement in the process of bone healing, and then improve the initial stability of the implant.[11−13] On the other hand, this structure can provide a large specific surface area and expose more active sites for protein absorption and osteoblast spreading.[14] Studies have shown that the local osteogenic microenvironment can be regulated by bioactive ions released from bioactive modified bone implants under the process of physicochemical dissolution, hydrolysis, and enzyme corrosion.[15] Ca ions have a strong affinity with phosphatidylserine (a phospholipid membrane component), which can promote biomineralization by accelerating the early formation of bonelike apatite, and further enhance the adsorption of fibronectin, improve cytological behavior, and finally promote new bone formation.[16] While P-containing groups can not only release specific signals to induce osteogenic differentiation but also provide the calibration site-specific adsorption of Ca ions to form calcium phosphate, the main inorganic component of bone.[17,18] Therefore, introducing bioactive elements of Ca and P into the porous Ti alloy scaffold simultaneously and constructing the micro/nano multistage structure have often been reported to mimic natural bone tissue structurally and compositionally.[19]

Some linear surface modification methods such as plasma spraying and ion implantation are difficult to process 3D porous matrix with complex shape, which makes the surface modification of 3D porous metals more challenging.[20−22] The hydrothermal technique (HT) has been successfully used in our previous study to form a uniform Ca-doped TiP coating with micro/nanoscaled hierarchical network topography at high temperatures and high pressures.[4] In the past decade, the microarc oxidation (MAO) technique, under the action of instantaneous high temperatures and high pressures produced by arc discharge, has often been applied to fabricate ceramic coatings with micro/nanoporous structure mainly composed of oxides and supplemented bioactive elements Ca and P with Ca/P ratios close to bonelike apatite by adjusting the ratio of Ca and P salts in the electrolyte on the surface of Ti alloy.[23,24] However, both treatments can form a structure/component bionic coating on the surface of Ti alloy, which one possesses better osteogenic properties has not been determined.

In this study, we compared the micro/nanomorphology, elemental component, and phase composition of HT and MAO coatings on the surface of 3D printed porous Ti6Al4V (Ti64) scaffolds and also investigated the *in vitro* effects of HT and MAO coatings on osteoblast adhesion, proliferation, differentiation, mineralization, and apoptosis. Then, we explored the bone binding of the three kinds of scaffolds in a rat skull defect model and identified the intraosseous growth pattern and bone/implant interface characteristics of the scaffolds treated with HT and MAO.

2. RESULTS AND DISCUSSION

2.1. Physical and Chemical Characterization of Micro/Nanocoatings.
The surface properties of implant materials, including surface morphology and chemical elements, directly affect the biological behaviors of osteoblasts, such as adhesion, proliferation, and differentiation, and ultimately affect the

stability and success rate of the implant.[25,26] The inspiration of this study came from the fact that the inorganic component of natural bone trabeculae is mainly composed of calcium (Ca) and phosphorus (P), with a micro/nano hierarchical structure. According to the principle of bionics and *in situ* doping of calcium, microspheres with nanoneedles and bioactive coatings with micro/nano hierarchical pore structures were prepared on the surface of Ti64. Stereomicroscopy showed that interconnected regular pores uniformly distributed in the 3D printed Ti64 scaffold (Figure 1A). For the H-Ti scaffold
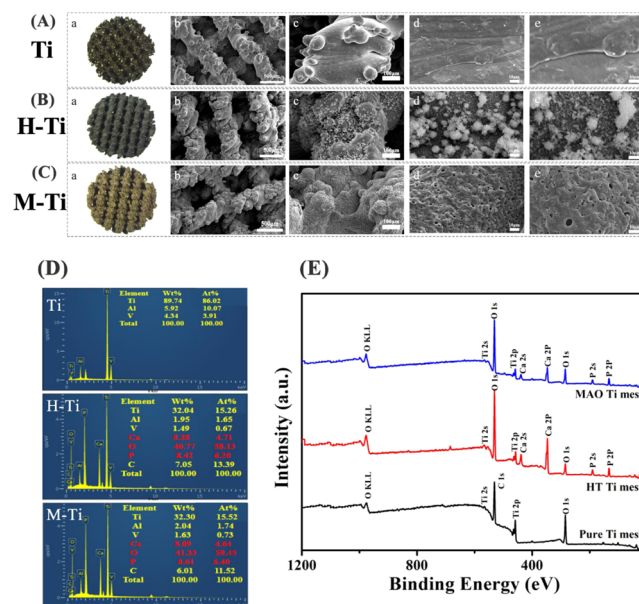
Figure 1. (A-a) Ti64 scaffold (Ti), (B-a) scaffold treated by the hydrothermal method (H-Ti), and (C-a) scaffold treated by the microarc oxidation method (M-Ti); (A-b−e; B-b−e; C-b−e) SEM surface morphologies of Ti, H-Ti, and M-Ti. (D) Energy-dispersive spectrometry (EDS) elemental analysis on the surfaces of three groups. (E) XPS analysis of three groups.

(Figure 1B), the surface was evenly covered with a black coating, and the 3D porous structure was still visible. However, the surface of the M-Ti porous scaffold was covered with a brown coating (Figure 1C). The scanning electron microscopy (SEM) images of the three groups show that the surface of the Ti group is relatively flat, and there is no specific nanoscale structure (Figure 1A-e). The surface of the H-Ti group has many microspheres consisting of nanorods, which grow radially from the surface, and also disperses some deposits caused by the crystallization of the remaining elements such as P and Ca in the solution (Figure 1B-b−e). Through the MAO process, the 3D printed scaffold also displays micro/nano multilevel porous morphology and a bioactive CaP coating has formed on the surface (Figure 1C-b−e).

Compared with the surface roughness, the chemical compositions of the coating play more important roles in cell adhesion. At present, it is believed that chemical components can directly activate related signal pathways, resulting in changes in the structure of the cell membrane across proteins, thus increasing protein adsorption and promoting osteoblast adhesion to the implant surface.[27] EDS analysis (Figure 1D) shows that the coating on the surface of the scaffold has a high Ca/P ratio, which is similar to that of bone apatite. The chemical compositions and states of each element in the three
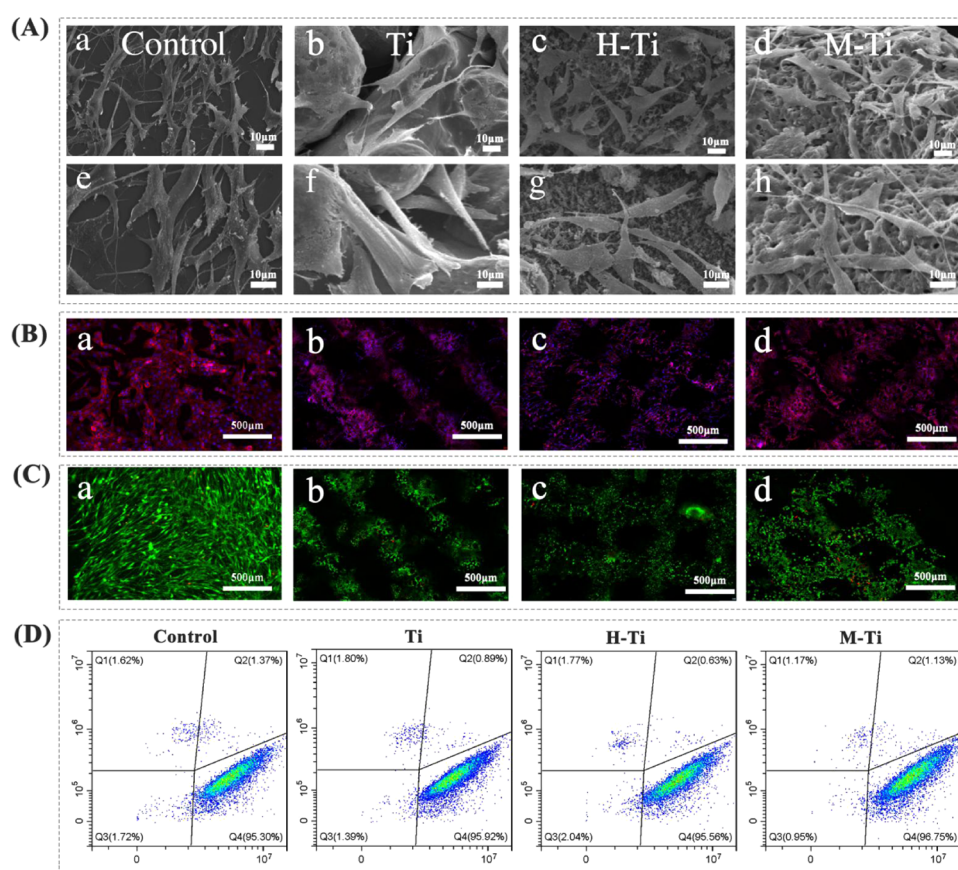
Figure 2. (A) SEM images of the adhesion and spreading of osteoblasts cultured for 3 days, (B) confocal laser scanning microscopy (CLSM) of actin (red) and nucleus (blue) on the samples cultured for 3 days, (C) live/dead fluorescence staining of cells cultured for 3 days, and (D) cell viability was analyzed by flow cytometry. a, e, control; b, f, Ti group; c, g, H-Ti group; and d, h, M-Ti group. There was no significant difference in the percentage of living and dead cells among the four groups.

groups were further studied by XPS (Figure 1E), and it is obvious that in comparison to the control group, both surfaces of H-Ti and M-Ti groups are mainly composed of O, Ti, Ca, and P elements, implying that Ca, O, and P elements have been successfully incorporated into the surface coating.

2.2. In Vitro Cell Behavior. 2.2.1. Cell Adhesion. It is important to study the adhesion and migration of osteoblasts on the surface of implant materials. Recent studies have shown that the appropriate surface roughness of the implant, especially the micro/nano surface morphology, provides good three-dimensional space for the cells and increases the hydrophilicity of the material surface, thereby promoting the adhesion of osteoblasts.[28,29]

We used SEM images to observe the adhesion and migration of MC3T3-E1 osteoblasts cultured in three groups for 3 days (Figure 2A). The treated Petri dish is most suitable for cell adhesion and is used as the control group (Figure 2A-a,e). The osteoblasts on different surfaces showed completely different morphologies. In the Ti group, cells formed a shallow monolayer dispersed only on the surface and extended a small number of cellular pseudopodia (Figure 2A-b,f). In the H-Ti group, polygonal or spindle cells increased and pseudopodia increased (Figure 2A-c,g). In the M-Ti group, the number of osteoblasts increased significantly compared with the first two groups, showing multiple connecting pseudopodia (Figure 2A-d,h). Previously, it has been reported that an anodically oxidized dental implant exhibited bone/implant interlocking after intraosseous implantation.[30] How-

ever, bone bonding on the flat surface of the MAO-treated implant is unsatisfactory. Therefore, the micro/nano multilevel pores generated in our studies are expected to contribute significantly to the generation of stronger bonding strength.

In line with the SEM results, the CLSM images showed that osteoblasts on the two modified samples (H-Ti and M-Ti group) exhibited more increasing number of osteoblasts and more clearly cytoskeletons to the control (Petri dish) and pure Ti as confirmed by actin staining (Figure 2B-a–d). It was believed that the chemical components directly activate the relevant signal pathways, resulting in changes in the structure of cell membrane transmembrane proteins and thus increasing the adsorption of proteins on the implant surface and promoting cell adhesion and proliferation on the implant surface. The micro/nanocoatings of the M-Ti group and H-Ti group were mixed with appropriate amounts of calcium, oxygen, and phosphorus ions, which were the same as the main components of bone apatite. The continuous release of ions changes the extracellular pH of osteoblasts, resulting in variations in the structure of transmembrane proteins, which is conducive to the binding of osteoblasts to plasma proteins adsorbed on the surface of the micro/nanocoating. The multipolar pore structure of the M-Ti group could further increase the surface roughness, hydrophilicity, and specific surface area of the implanted materials, which can theoretically increase the integrin-binding sites and plasma protein absorption rate.
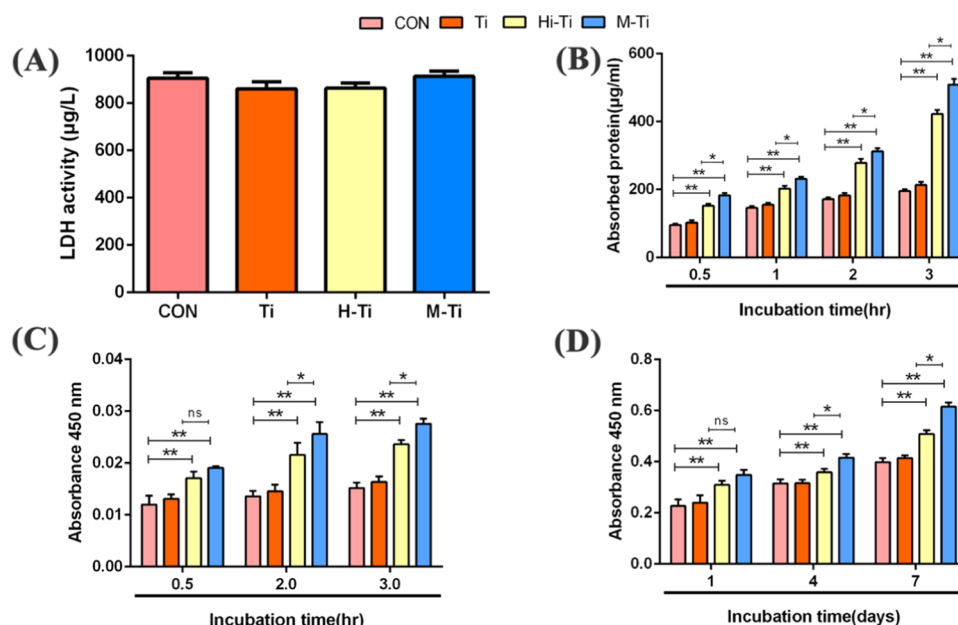
Figure 3. (A) Lactate dehydrogenase (LDH) activity released during the first 3 days of incubation; (B) amount of total protein adsorbed at 0.5, 1, 2, and 3 h of culture in each group; (C) cell adhesion measured by the CCK-8 assay after 0.5, 2, and 3 h of culture; and (D) cell proliferation measured by the CCK-8 assay after 1, 4, and 7 days of culture. $**p < 0.01$ compared to control and Ti groups, $* p < 0.05$ compared to the H-Ti group.
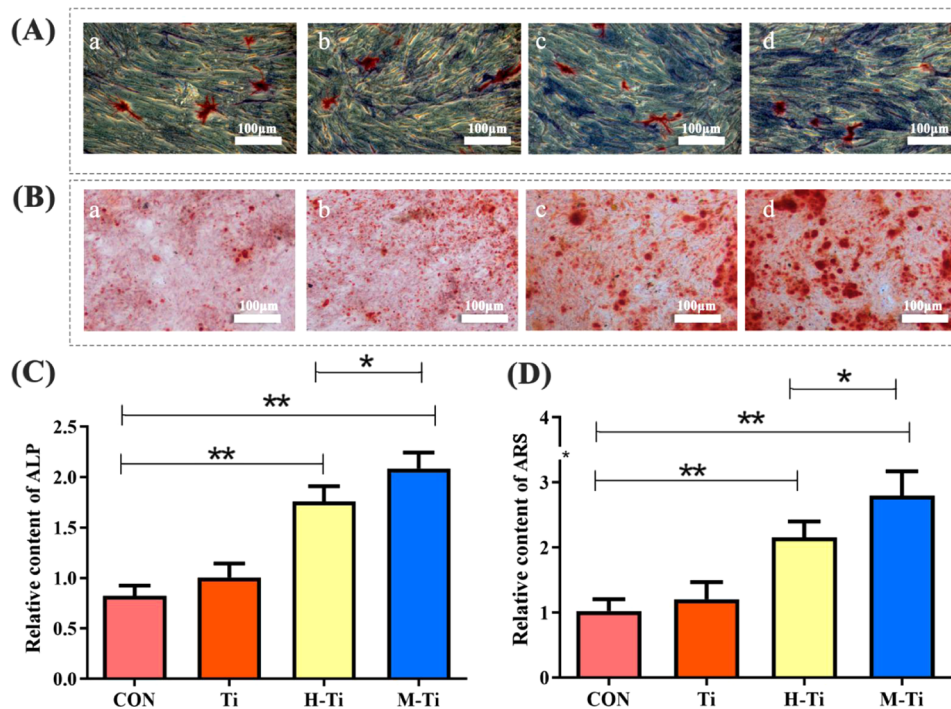
Figure 4. a, Control; b, Ti group; c, H-Ti group; and d, M-Ti group. (A) ALP generated by cells cultured on different samples and results after culturing for 7 days and (C) ALP relative content. (B) ECM mineralized nodules generated by cells cultured on different samples after culturing for 15 days and (D) ECM relative content. There are significant differences between H-Ti and M-Ti compared with the control group and Ti group, and there are differences between H-Ti and M-Ti groups. $**p < 0.01$ compared to control and Ti groups, $* p < 0.05$ compared to the H-Ti group.

2.2.2. Cytocompatibility.
The cytotoxicity test is the most commonly used method to evaluate the biocompatibility of biomaterials. There are many methods to evaluate the cytotoxicity of biomaterials, including cell morphology, cell growth ability, cell cycle, and apoptosis. In this study, the cytotoxicity of the Ti group, H-Ti group, and M-Ti group was evaluated by live/dead fluorescence staining, flow cytometry, and CCK-8 test.

After osteoblasts were cultured for 3 days, the activity and morphology of osteoblasts on these scaffolds were evaluated by live/dead fluorescence staining (Figure 2C). Compared with the control group, there was no significant decrease in the number of living cells in the Ti group, H-Ti group, and M-Ti
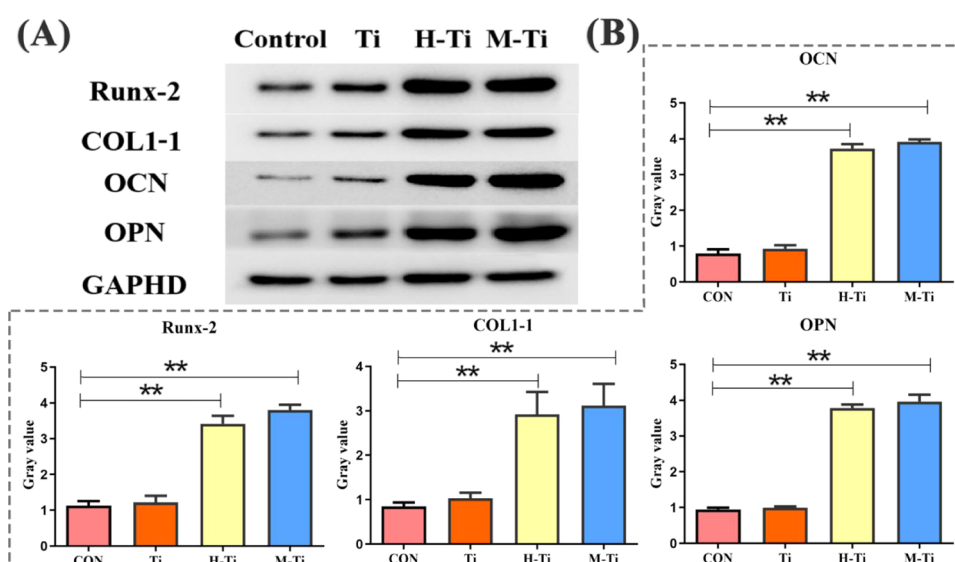
Figure 5. Western blot assay analysis qualitatively (A) and quantitatively (B) on Runx-2, COL1A1, OCN, and OPN for detecting osteoblastic differentiation. **$p < 0.01$ compared to control and Ti groups, *$p < 0.05$ compared to the H-Ti group.
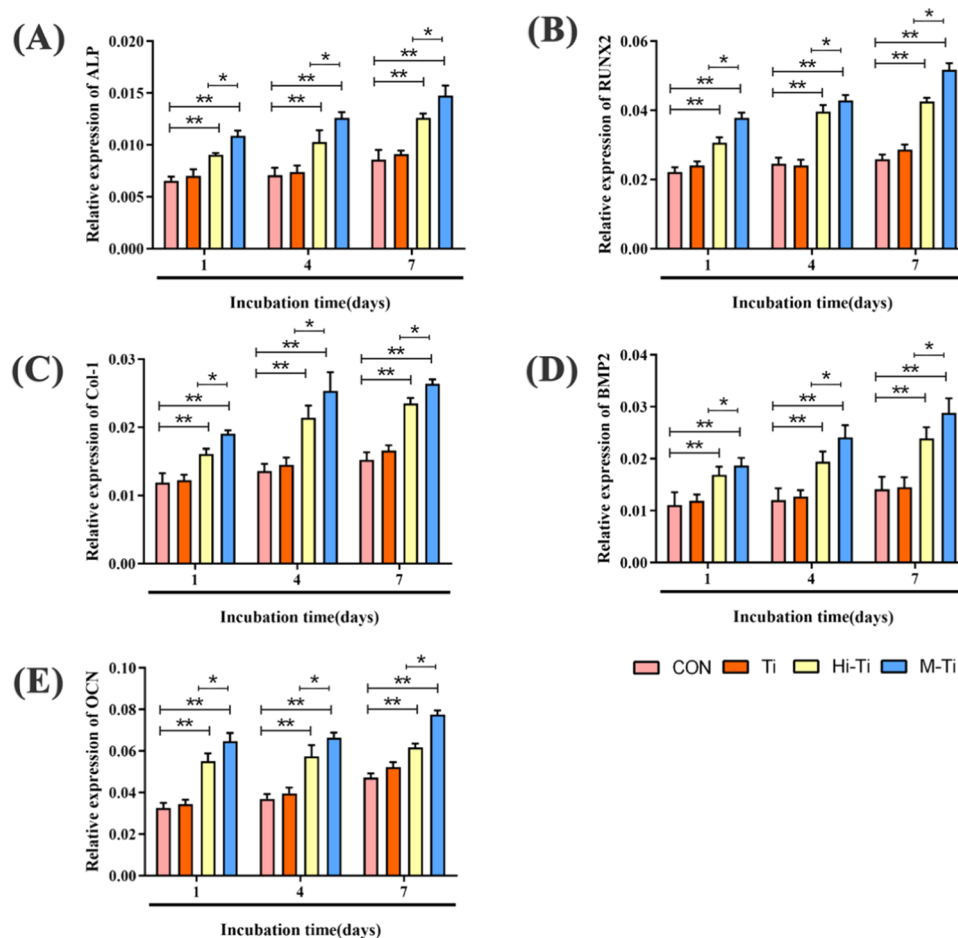
Figure 6. mRNA expression levels of ALP (A), RUNX-2 (B), COL-1 (C), BMP-2 (D), and OCN (E) in osteoblasts cultured for 1, 4, and 7 days, detected by qRT-PCR. **$p < 0.01$ compared to control and Ti groups, *$p < 0.05$ compared to the H-Ti group.

group. The results of flow cytometry showed that there was no significant difference in the percentage of living and dead cells among the four groups (Figure 2D).

Lactate dehydrogenase (LDH) activity and protein adsorption are also important indexes to evaluate the

cytotoxicity of materials. The activity of LDH was similar among different groups (Figure 3A). Ca, O, and P ion coating did not increase the level of cytotoxicity, which was consistent with the results of flow cytometry. Protein adsorption behavior is closely related to surface properties, especially to surface
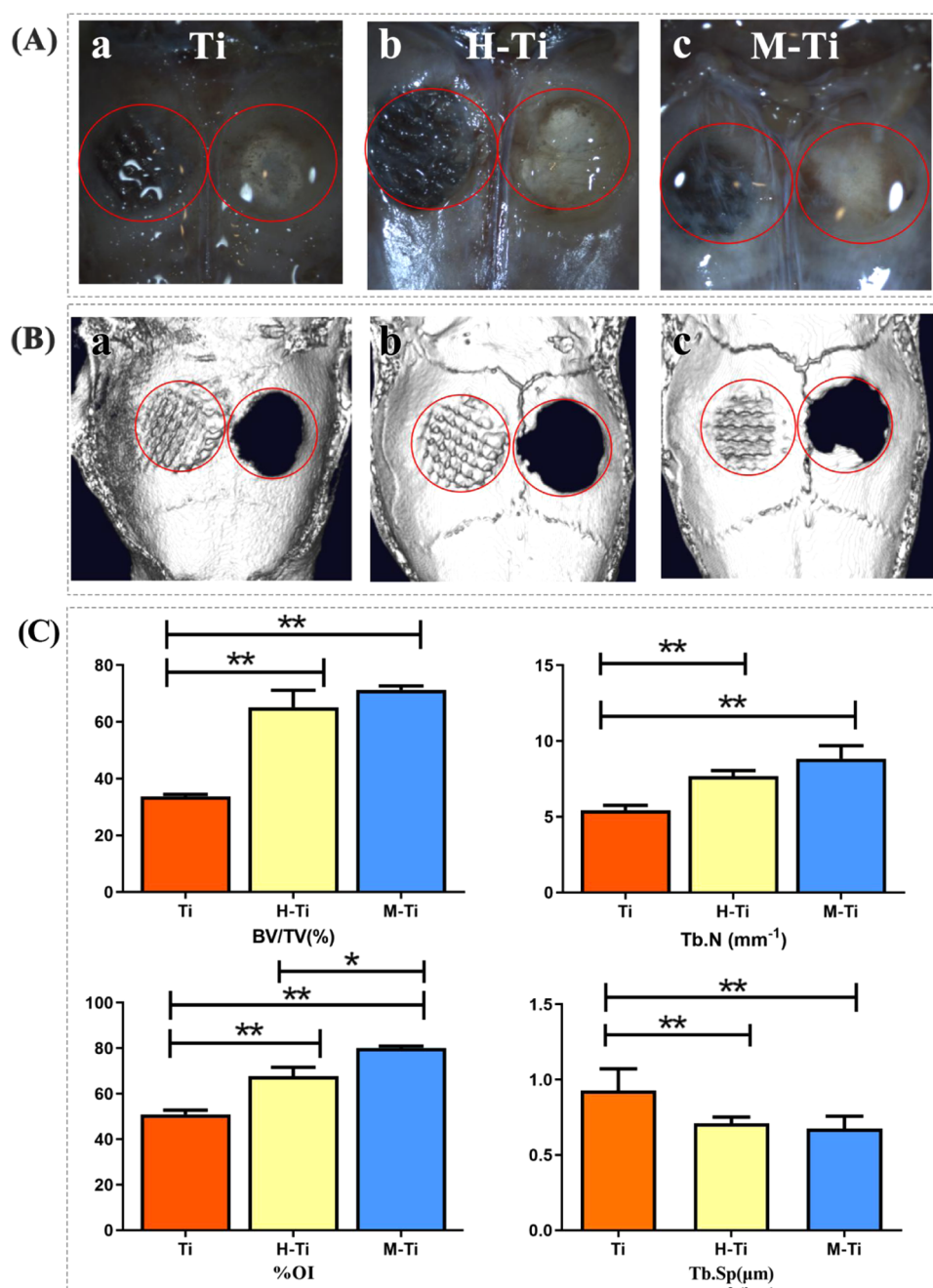
Figure 7. a, Ti group; b, H-Ti group; and c, M-Ti group. (A, B) Gross observation and μ-CT images of the bone−implant interface at 12 weeks postimplantation. (C) Quantitative analysis of osseointegration for μ-CT results. $**p < 0.01$ compared to control and Ti groups, $*p < 0.05$ compared to the H-Ti group.

roughness. As shown in Figure 3B, the amount of proteins adsorbed on the surface gradually increased with time by different samples. The protein absorption of both M-Ti and H-Ti groups was significantly higher than that of the Ti group and control group at every time point, indicating that the coating on the modified Ti surfaces (H-Ti and M-Ti group) promoted protein adsorption.

The adhesion and proliferation of osteoblasts on the surface of the control group, Ti, H-Ti, and M-Ti group were further evaluated by the CCK-8 assay. As shown in Figure 3C, the number of adherent cells in the M-Ti group and H-Ti group was significantly higher than that in the control group and Ti group. Figure 3D shows the proliferation of osteoblasts on the

surface of different samples at various time points. In general, cell proliferation in different groups gradually increased over time. In comparison with the control and Ti groups, cell proliferation in the H-Ti and M-Ti groups was significantly higher. The results indicated that the modified surface structures and the slow release of Ca, O, and P ions from the coatings promoted cell adhesion and proliferation. In addition, protein adhesion and proliferation in the M-Ti group was higher than that in the H-Ti group at different time points, showing that the micro/nanoporous scaffold coating with MAO treatment can provide necessary adhesion conditions and physical structure for cell growth and migration. In short, the micro/nanotextured hierarchical biomimetic topography
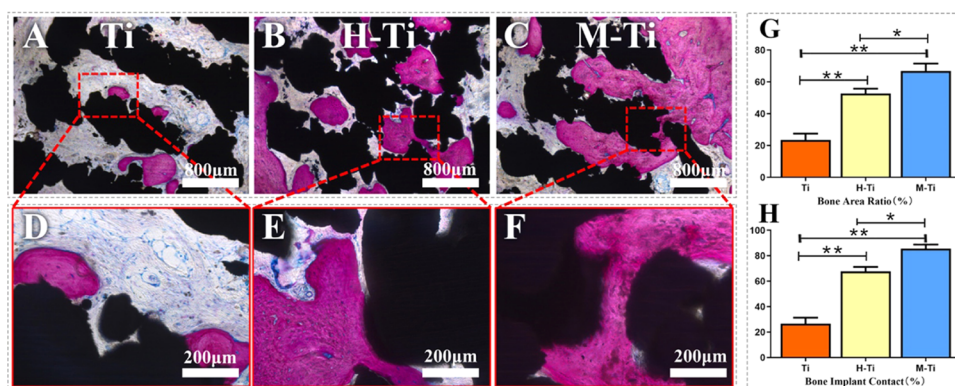
Figure 8. Histological observation of Ti group (A), H-Ti group (B), and M-Ti group (C). (D−F) Magnified images of the selected region corresponding to (A−C), respectively. Quantitative results of bone ingrowth (G) and bone−implant contact ratio (H) of the three experimental groups. **$p < 0.01$ compared to control and Ti groups, *$p < 0.05$ compared to the H-Ti group.

with Ca, O, and P ions could enhance the adhesion and proliferation ability of osteoblasts.

2.2.3. Osteogenic Activity. The modified surface structures and the release of Ca, O, and P ions are expected to promote the osteogenic differentiation of osteoblasts on the scaffold. The expression level of alkaline phosphatase (ALP) was used as an early marker and alizarin red staining was used to detect extracellular matrix (ECM) mineralization. As shown in Figure 4A,C, the staining of ALP in the H-Ti group and M-Ti group was significantly higher than that in the Ti group and control group. For alizarin red staining (Figure 4B,D), all samples showed mineralized nodules (red). However, the number of mineralized nodules in the H-Ti group and M-Ti group was significantly higher than that in the Ti group. Furthermore, the number of mineralized nodules in M-Ti group was higher than that in the H-Ti group. These results indicated that the micro−nanocoating of the H-Ti group and M-Ti group can promote the mineralization of osteoblasts. In addition, the multistage pore structure of the M-Ti group is more conducive to the fine growth and differentiation of osteoblasts.

2.2.4. Protein and Gene Expression of Osteogenic Markers. It is widely known that osteogenic differentiation associates with the expression levels of proteins. Runx-2 is a specific transcription factor, which plays an important role in osteoblast differentiation, cytotoxicology, and osteogenic maturation.[31] OCN and OPN appear in the late stage of osteoblast differentiation and regulate the growth of hydroxyapatite (HA) crystals.[32] Collagen type I (Col-1) protein is the main type of collagen in bone tissue with the reticular structure, which plays a key role in maintaining the integrity of the bone structure. Here, the differentiation of osteoblasts on Petri dish, pure Ti, H-Ti, and M-Ti was detected through the expression of Runx-2, Col-1, OCN, and OPN by the western blot assay. As shown in Figure 5, significant upregulation of Runx-2, Col-1, OCN, and OPN was observed for H-Ti and M-Ti groups compared with that for control and pure Ti groups. However, there was no significant difference between the H-Ti and M-Ti groups. The observed phenomenon is consistent with the quantitative results of the gray values of each protein band (Figure 5). The mRNA expression of ALP, Runx-2, Col-1, BMP-2, and OCN was assessed by real-time polymerase chain reaction (PCR) after culturing for 1, 4, and 7 days, and the results are provided in Figure 6. At various time points, these osteogenesis-related genes were significantly upregulated in the modified samples when compared with the control and

pure Ti groups. The M-Ti group showed stronger osteogenesis enhancement compared with the H-Ti group. These results indicated that the surface topography could influence the osteoblast osteogenesis and the release of Ca, O, and P ions played an indispensable role.

2.3. *In Vivo* Implantation. *2.3.1. μ-CT Analysis.* To explore the effect of HT/MAO treatment and Ca, O, and P deposition on the *in vivo* osseointegration of the porous Ti64 scaffold, the scaffold was implanted into the rat calvarial bone defect for 12 weeks; by then, bone remodeling has already occurred. To eliminate the interference of individual differences of different experimental animals, the cavity of the same size was taken as the control group in the contralateral position of the skull bone. In general, there was no infection, osteolysis, and necrosis. As shown in Figure 7A, the Ti group, H-Ti group, and M-Ti group were covered by dense white tissue, and the injury boundary disappeared. Only a transparent membrane was formed in the contralateral blank control group, and the injury boundary was still visible. The newly formed bone both around the scaffold and within it was quantified by μ-CT (Figure 7B,C). As shown, both the thickness and the area of newly formed bone for H-Ti and M-Ti groups were much larger than those for the Ti group. There was a certain bone connection between the M-Ti scaffold and surrounding bone tissue, the new bone tissue was significantly increased, and the surrounding bone tissue was dense. Quantitative analysis demonstrated that both modified implants (H-Ti and M-Ti group) have markedly increased BV/TV ($p < 0.01$), Tb.N ($p < 0.05$), and %OI ($p < 0.01$) and decreased Tb.sp ($p < 0.01$). Meanwhile, there was no significant difference between H-Ti and M-Ti groups except for %OI.

2.3.2. Quantitative and Qualitative Histological Results. Figure 8 shows the representative histological images of cross-sectioned implants in the calvarial bone defect. The pillars of the implants are shown in black, while the mineralized trabeculae are shown in red. New bone tissue could be seen around the implants in all three groups. For the pure Ti group, only the peripheral area is deposited by mineralized bones (Figure 8A,D). In contrast, the bone ingrowth in the H-Ti group (Figure 8B,E) and the M-Ti group (Figure 8C,F) is more extensive and even bridged the adjacent pillars. The result demonstrates that Ca, O and P elements associated with the modified surface coating change the extracellular environment and have a better osteogenic effect. Compared with the H-Ti group, the mature trabecular bone in the M-Ti group is

Table 1. Reaction Conditions Used in This Study

reactants	reaction conditions	sample name	acronym
Ti64 powder	3D printing	porous Ti64 scaffold	Ti
mH_2O_2/mH_3PO_4 =9:1 0.2 g/mL CaCl$_2$	220 °C, 24 h 120 °C, 8 h	two-step hydrothermally treated Ti64 scaffold	H-Ti
0.065 M Ca(CH$_3$COO)$_2$·H$_2$O, 0.03 M NaH$_2$PO$_4$, 0.065 M EDTA-2Na, 0.5 M NaOH	350 V, 500 Hz, 10%, 5 min	microarc oxidation-treated Ti64 scaffold	M-Ti

more closely connected with the micro−nanocoating on the surface of the three-dimensional scaffold. Quantitative analysis shows that implants with the modified surface (H-Ti and M-Ti groups) have significantly boosted histomorphometric parameters and that the M-Ti surface demonstrated the most significant bone-healing effects.

The osseointegration ability of the pure titanium scaffold without surface modification is insufficient. Similar to previous studies, the bone area ratio is generally 20−30%.[33−35] Previous studies have fully demonstrated that the modified surface coating of Ti by both MAO and the HT method could enhance bone formation and osseointegration.[5,13,36] The same phenomenon has been also observed from our results. However, the micro/nano hierarchical porous coating prepared by MAO seems to have better performance with a higher bone area ratio and bone−implant contact. It might have resulted from the multiple micropores on the MAO surface coating. Xiu et al. has shown that numerous globular bone matrixes with a diameter of 1−2 μm were specifically located in the micropores on the bone−implant surface.[6] That might provide an anchorage point between scaffolds and new formation bone tissue through a microporous structure and further promote the natural bone remodeling and implant osseointegration.[37−39]

3. CONCLUSIONS

To improve osseointegration, we used the hydrothermal technique and microarc oxidation technique to modify 3D printed porous Ti64 scaffolds by the incorporation of biomimetic Ca, O, and P elements for obtaining micro/nanocoatings with different morphologies. The modified samples (H-Ti and M-Ti groups) show moderate surface roughness, improved biocompatibility, and enhanced osteogenesis capability. Compared with the hydrothermal surface treatment, MAO surface treatment shows better biocompatibility and osteogenesis capability. Besides, both *in vitro* and *in vivo* studies indicated that the introduction of Ca, O, and P ions could significantly promote osteoblast adhesion/proliferation and further accelerate the maturation and mineralization of osteoblasts. Thus, the Ca-, O-, and P-doped Ti implant with the MAO surface coating is a much better candidate with the great potential to be used in orthopedic applications.

4. MATERIALS AND METHODS

4.1. Materials and Methods. *4.1.1. Preparation of Three-Dimensional (3D) Printed Porous Ti6Al4V Alloy Scaffolds.* It is reported in the previous studies that macropores in the range of 100−400 μm can promote the ingrowth of bone and blood vessels, and the pore size recommended for cell ingrowth was approximately 100−300 μm.[40,41] So, we 3D printed the Ti6Al4V scaffold with a pore size of 300 μm in the study. First, software of material/magics was used to construct a porous titanium alloy scaffold model with a porosity of 300 μm and a size of φ 5 mm × 5 mm.

Then, we 3D printed porous Ti6Al4V (Ti64) scaffolds using a Swedish Arcam (AL) electron beam rapid prototyping system that lays the forming substrate flat on the power bed; afterward, the medical Ti-6Al-4V (ELL) alloy powder with a chemical composition of Ti89.22, Al6.88, and V3.90 (wt %) with an average particle size of 50 μm in the powder feeding cylinder is evenly spread on the substrate of the forming cylinder with a powder spreading rake. Each newly laid powder layer is prescanned several times by electron beam at a certain scanning rate, and the powder layer is preheated to about 730 °C. Then, the preheating layer is melted and scanned once. According to the information of the section outline of the first layer set by the CAD model, some areas of the powder layer are selectively sintered to form a horizontal two-dimensional section of the part. Then, the piston of the forming cylinder drops a certain distance, the piston of the powder supplying cylinder rises the same distance, the powder is smoothened again by the powder spreading rake, and the electron beam begins to scan the powder according to the CAD information of the second layer of the part. This is repeated layer by layer until the sample preparation is complete, followed by ultrasonic cleaning with acetone, ethanol, and deionized water, respectively. Of note, the raw material of Ti-6Al-4V (ELL) alloy powder with a chemical composition of Ti89.22, Al6.88, and V3.90 (wt %) with an average particle size of 50 μm is of medical grade. Here, the raw materials and equipment were provided by Shenyang Institute of Metals, Chinese Academy of Sciences.

4.1.2. Synthesis of Coatings. 4.1.2.1. Hydrothermal (HT) Treatment. The 3D printed porous Ti64 scaffold was immersed in a mixed aqueous solution of H$_2$O$_2$ and H$_3$PO$_4$ at a mass ratio of 9:1, then subjected to a hydrothermal reaction in a Teflon-lined autoclave under 220 °C for 24 h, and transferred into 0.2 g/mL CaCl$_2$ solutions to introduce the Ca element in a Teflon-lined autoclave at 120 °C for 8 h.

4.1.2.2. Microarc Oxidation (MAO) Treatment. The 3D printed porous Ti64 scaffold was used as an anode and a stainless steel plate as a cathode. The MAO process was carried out in an aqueous electrolyte containing 0.065 M calcium acetate monohydrate (Ca(CH$_3$COO)$_2$·H$_2$O), 0.03 M sodium dihydrogen phosphate (NaH$_2$PO$_4$), 0.065 M ethylenediamine tetraethylenediamine (EDTA-2Na), and 0.5 M sodium hydroxide (NaOH). During which, the working voltage was 350 V, the pulse frequency was 500 Hz, the duty cycle was 10%, the reaction time was 5 min, and the bath temperature was maintained below 40 °C by cooling water. The detailed reaction conditions are listed in Table 1 as below.

4.2. Surface Characterization. The surface morphologies of all samples were observed by field-emission scanning electron microscopy (SEM, Eindhoven), and the surface element composition was determined by energy-dispersive X-ray spectroscopy (EDS, EPMA, JAX-8100, Japan). The chemical states of titanium (Ti), oxygen (O), and phosphorus (P) were analyzed by X-ray photoelectron spectroscopy (XPS). The data were analyzed by XPS Peak Fit 4.1 software.

4.3. In Vitro Studies. *4.3.1. Cell Culture.* Mouse osteoblast line MC3T3-E1 obtained from Sichuan University, China, Sichuan University Cell Bank was used in this study. MC3T3-E1 cells were cultured in high-glucose Dulbecco's modified Eagle's medium (DMEM, HyClone) with 10% fetal bovine serum (FBS, HyClone) and 1% antimicrobial solution of penicillin and streptomycin at 37 °C in a humidified atmosphere of 5% CO_2. The medium was changed every 3 days, and the growth morphology of MC3T3-E1 was observed by an inverted phase-contrast microscope when the cells reached 80−90% confluence and then passaged. Only the third passage (P3) cell was applied in all in vitro experiments.

4.3.2. Cell Attachment Assay. Ti, H-Ti, and M-Ti scaffolds were sterilized with a low-temperature plasma sterilizer (hrpa-120, Haier, Qingdao, China). Before inoculating the cells, each material was soaked in DMEM for 12 h to make it thoroughly moist. In total, 1×10^4 P3 MC3T3-E1 cells were cocultured with each group of samples (Ti, H-Ti, and M-Ti) in a 24-well culture plate with 2 mL of culture medium. Three parallel samples in each group. The cells were cultured with 5% CO_2 in a humidity incubator at 37 °C for 72 h. After that, the samples were taken out and washed with phosphate-buffered saline (PBS) to wash away unattached cells. The remaining cells on the samples were fixed with 2.5% glutaraldehyde, dehydrated in a series of ethanol solutions (20, 40, 60, 80, 90, and 100%), and then gold-sputtered for SEM (scanning electron microscope JSM-6510LV, JEOL, Japan) analysis.

4.3.3. Cell Cytoskeleton Staining. The P3 MC3T3-E1 cells were inoculated with Ti, H-Ti, and M-Ti samples at a density of 1×10^4 cells/well. Each group has three parallel samples. After 72 h coculture, the remaining cells on the samples were permeated with 0.2% Triton X-100 (Sigma-Aldrich) for 15 min, cell nuclei were stained with 4′,6-diamidino-2-phenyl-indole (DAPI), and the cytoskeletons were stained with rhodamine-conjugated phalloidin for 20 min. Then, the cell cytoskeleton was observed by confocal laser scanning microscopy (CLSM, Nikon, Japan). The parameters of the laser scanning microscope are as follows: the laser is a semiconductor solid-state laser; the output wavelength is 488, 550 nm, etc.; the Z-axis step is 1.0 μm; the scanning mode is the XYZT scanning mode; and the scanning speed is slow. After prescanning, the best scanning parameters were determined, the bottom of the sample was focused, and the computer scanned continuously along the Z-axis of the sample through a microstepper motor to obtain the fluorescence image of each layer. A high-resolution multilayer overlay image was obtained. The collected images were processed by Olympus software.

4.3.4. Live/Dead Fluorescence Staining. Cell preparation and coculture with three parallel Ti, H-Ti, and M-Ti samples are the same as those in the cell attachment assay. According to the manufacturer's instructions, the cell viability was quantified using the Live/Dead stain (L34957, Invitrogen), and the cells were observed and photographed using a confocal laser scanning microscope.

4.3.5. Flow Cytometry. In a 24-well culture plate, three parallel Ti, H-Ti, and M-Ti samples in each group were cocultured with 1×10^4 P3 MC3T3-E1 cells. After 3 days, the cocultured cell suspension from the plate and scaffolds were collected and placed in the flow detection tube. After centrifugation, the culture medium was discarded and the cell viability was detected by flow cytometry. In brief, after the cells were washed using cold phosphate-buffered saline (PBS),

they were resuspended in a buffer without any visible aggregation of the cells. Then, Calcein-AM (CAM) (5 μL) and phosphatidylinositol (PI) (5 μL) were added, and the samples were incubated in the dark for 20 min at 37 °C. Live cells (Calcein positive, PI negative) were detected in the fourth quadrant (Q4), while dead cells (Calcein negative, PI positive) were detected in the first quadrant (Q1). The cells in the second quadrant (Q2, calcitonin positive, PI positive) represent cells with the permeable cytoplasmic membrane, that is, permeable cells, because PI is excluded by the cells with intact cytoplasmic membrane and enters the cells through the damaged and permeable cytoplasmic membrane. The third quadrant (Q3) is generally impurities or fragments in the sample. The more the points in the fourth quadrant (Q4) and the larger the ratio, the better the cell viability.

4.3.6. Lactate Dehydrogenase (LDH) Activity Assay. Lactate dehydrogenase (LDH) activity was used as an index of cytotoxicity. The samples were placed in 24-well plates with three wells in each group. In total, 1×10^4 P3 MC3T3-E1 cells were seeded in each well. After 72 h of cell culture, the culture medium was collected and centrifuged for the determination of LDH activity using an LDH activity detection kit (ab102526, Abcam, U.K.). LDH activity was determined spectrophoto-metrically (at 440 nm) according to the manufacturer's instructions

4.3.7. Protein Adsorption Analyses. The protein adsorption capacity of different coatings was evaluated by fetal bovine serum (FBS) adsorption analyses. Three parallel samples were placed in a 24-well culture plate in each group and 2 mL of 10% FBS/DMEM was added to each well, followed by incubation at 37 °C for 24 h. The plate was then rinsed with PBS, and 1% sodium dodecyl sulfate (SDS) solution was used to elute surface proteins. Protein concentration in the eluent was measured using a bicinchoninic acid (BCA) protein assay kit (ab102536, Abcam, U.K.).

4.3.8. Cell Adhesion and Proliferation Assay. In the cell adhesion assay, the preparation and incubation of cells are similar to those in the cell attachment assay. Three parallel samples of each group were cocultured with the same number of cells. After the different coculture time points of 0.5, 2, and 3 h, the samples were transferred in a new well with additional 24 h culture and the culture medium for examination. In the cell proliferation assay, cell preparation and incubation are similar to those in the LDH activity assy. Each group has three parallel samples. After different time points of cell culture of 1, 4, and 7 days, the culture medium was collected for detection. The adhesion and proliferation activities of MC3T3-E1 osteoblasts were measured using a CCK-8 kit (ab228554, Abcam, U.K.). The CCK-8 solution (20 μL) and 180 μL of serum-free culture medium were added to each well and then incubated for 2 h at 37 °C. Finally, the absorbance of the culture medium was determined by a Thermo microplate analyzer at 450 nm (Thermo). The serum-free DMEM medium was selected as the blank solution to optimize the absorbance. The material in control group is coverslip.

4.3.9. Osteogenic Activity Evaluation. Three parallel Ti, H-Ti, and M-Ti samples in each group were cocultured with 1×10^4 P3 MC3T3-E1 cells in a 24-well culture plate. Cells directly cultured on the well plate was selected as the control group. After 24 h coculture, the culture medium was changed with osteoinduction medium: a normal culture medium containing 10 μL/mL β-glycerophosphate, 50 μg/mL ascorbic acid, and 10 μL/mL dexamethasone. After 7 days of

Table 2. Primers Used for qRT-PCR

gene	foward primer sequence (5′−3′)	reverse primer sequence (5′−3′)
ALP	AACGTGGCCAAGAACATCATCA	TGTCCATCTCCAGCCGTGTC
OCN	GGTGCAGACCTAGCAGACACCA	AGGTAGCGCCGGAGTCTATTCA
Col-1	GCCTCCCAGAACATCACCTA	GCAGGGACTTCTTGAGGTTG
BMP-2	CAACACCGTGCTCAGCTTCC	TTCCCACTCATTTCTGAAAGTTCC
RUNX-2	CCATAACGGTCTTCACAAATCCT	TCTGTCTGTGCCTTCTTGGTTC
GAPDH	GATGCTGGTG CTGAGTATGRCG	GGATCTTCATGAGGTAGTCA

osteoinduction culture, the cells only from the scaffolds were collected by a trypsin digestion method and transferred to a new well with additional 24 h osteoinduction culture. Cells were fixed and stained with an ALP kit (P0321M Beyotime, Shanghai, China), and the ALP was quantitatively analyzed by *p*-nitro phenyl phosphate (pNPP) (BP25341 Sigma-Aldrich) at the same time. The ALP activity was expressed as the optical density (OD) value at 405 nm per milligram of total protein. Calcium deposition was detected to verify the extracellular matrix mineralization ability of different samples. After being cultured in osteoinduction culture for 14 days, the cells only from the scaffolds were collected and transferred to a new well with additional 24 h osteoinduction culture. Calcium deposition assays were further performed. First, the cells were fixed with 70% ethanol and stained with 40 mM alizarin red S (ST1078 Beyotime, Shanghai, China) solution. Then, the staining "hole" was eluted with 10% cetylpyridinium chloride 1104006 (Sigma-Aldrich) solution, and OD values were measured at 590 nm for quantitative analysis. The results of calcium deposition were normalized by total protein content and were expressed as the OD value at 590 nm per milligram of total protein in the cells.

4.3.10. Western Blotting. The cell preparation and incubation are the same as those for the osteogenic activity evaluation. After 7 days of osteoinduction culture, the cells only from the scaffolds were collected by the trypsin digestion method. The cells purely cultured in a well plate were collected as the control group. Then, the collected cells and a cell lysis buffer were used for protein extraction. The protein concentration was determined, and then, the protein samples were heated, denatured, and analyzed by SDS-polyacrylamide gel electrophoresis (SDS-PAGE). Proteins on poly(vinylidene fluoride) (PVDF) membranes were separated by standard methods. The membrane was then sealed with 5% skimmed milk powder for 2 h and incubated overnight with mouse anti-COL1A1 (ab34710, 1:1000; Abcam, U.K.), rabbit anti-RUNX-2 (ab76956, 1:1000; Abcam, U.K.), rabbit anti-OCN (ab93876, 1:500; Abcam, U.K.), rabbit anti-OPN (ab8448, 1:1000; Abcam, U.K.), and GAPDH (ab263962, Abcam, U.K.) at 4 °C. After washing with Tris buffer, proteins on PVDF membranes were incubated with a secondary antibody at room temperature for 2 h. Determination of the protein content was done by enhanced chemiluminescence.

4.3.11. qRT-PCR. The cell preparation and incubation are the same as those for the osteogenic activity evaluation. The surface cells of the sample were collected using the TRIzol kit to extract the total RNA from each group. Three parallel samples were set up in each group, and nine samples from three culture plates were collected at the set time to obtain sufficient RNA. Using the Revert Aid TM First Strand cDNA Synthesis kit, mRNA was reverse-transcribed into cDNA, at 25 °C 10 min, 42 °C 50 min, and 85 °C 5 min, and the target genes were amplified by PCR; the information of PCR primers

is given in Table 2. The conditions of fluorescence quantitative PCR amplification are as follows: 94 °C 4 min, 94 °C 20 s, 60 °C 30 s, 72 °C 30 s, cycle 35 times, and signal detection at 72 °C. The relative content of expressed mRNA was expressed by the ratio of the target gene to internal reference GAPHD.

4.4. *In Vivo* Animal Study. *4.4.1. Construction of Calvarias Defect Models.* All animal operations were approved by the Animal Research Committee of West China Medical College of Sichuan University. A total of 36 male Sprague−Dawley rats (12 weeks old, weighing 350−400g) were selected. After the rats were anesthetized with isoflurane, a sagittal incision of 1.5−2.0 cm was made on the scalp. Electric ring drill (NouvagAG; Goldach, Switzerland) was used to create two full-thickness Φ 5 mm diameter defects (NouvagAG; Goldach, Swiss) on each side of the skull. Then, sterilized Ti, H-Ti, and M-Ti scaffolds with a diameter of 5 mm and a thickness of 2 mm were implanted in 18 cases in each group. Soft tissue reduction and suture with 4-0 silk thread were performed to achieve one-stage closure. Each rat received an intraperitoneal injection of antibiotics after the operation.

4.4.2. Micro-CT Evaluation (μ-CT). The implanted skulls were taken out at 12 weeks after the operation and scanned with a high-resolution μ-CT scanner (Sanco Medical μ-CT50). The scanning resolution was 18 μm. The collected images were reconstructed by software, and the three-dimensional model was reconstructed by the CT Vol program (Sky Scan Company). The bone volume per total sample volume (BV/TV), mean trabecular number (Tb.N), percentage of bone contact with implants (% Oi), mean trabecular separation (Tb.Sp) were calculated to determine the osteogenic characteristics of the implanted samples.

4.4.3. Histological Analysis. The implants and surrounding tissues were collected at 12 weeks after the operation. The samples were fixed with 4% paraformaldehyde, dehydrated by gradient ethanol, and embedded in poly(methyl methacrylate). The embedded samples were sliced with a diamond tissue slicer (SAT-001 Chengdu Aolijin), stained with methylene blue−acid fuchsin, and sealed with resin. The bone area ratio was defined as the percentage of mature bone within the whole tissue region (a ring region extending 250 μm from the implant surface). The bone-to-implant contact was defined as the percentage of the linear fraction of mineralized bone in direct contact with the implant interface based on the analysis using NIS-Elements F2.20 image software (Media Cybernetics).

4.4.4. Statistical Analysis. The data are expressed as the mean ± standard deviation (SD) from three independent experiments. The data were analyzed using SPSS 16.0 software (SPSS). One-way analysis of variance (ANOVA) followed by a Student−Newman−Keuls posthoc test was used to determine the level of significance. Values of $p < 0.05$ and 0.01 were considered to be significant and highly significant, respectively.

AUTHOR INFORMATION

Corresponding Authors

Ganjun Feng — *Department of Orthopedic Surgery and Orthopedic Research Institue, West China Hospital, Sichuan University, Chengdu, Sichuan 610041, China;* ◉ orcid.org/0000-0002-8945-8231; Email: gjfenghx@163.com

Limin Liu — *Department of Orthopedic Surgery and Orthopedic Research Institue, West China Hospital, Sichuan University, Chengdu, Sichuan 610041, China;* Email: 18980601394@163.com

Li Zhang — *Analytical and Testing Center, Sichuan University, Chengdu, Sichuan 610065, China;* Email: zhangli9111@126.com

Authors

Leizhen Huang — *Department of Orthopedic Surgery and Orthopedic Research Institue, West China Hospital, Sichuan University, Chengdu, Sichuan 610041, China*

Bianyun Cai — *College of Medical Technology and Engineering, Henan University of Science and Technology, Luoyang, Henan 471026, China*

Yong Huang — *Department of Orthopedic Surgery and Orthopedic Research Institue, West China Hospital, Sichuan University, Chengdu, Sichuan 610041, China*

Jingcheng Wang — *Department of Orthopedic Surgery and Orthopedic Research Institue, West China Hospital, Sichuan University, Chengdu, Sichuan 610041, China*

Ce Zhu — *Department of Orthopedic Surgery and Orthopedic Research Institue, West China Hospital, Sichuan University, Chengdu, Sichuan 610041, China*

Kun Shi — *Department of Orthopedic Surgery and Orthopedic Research Institue, West China Hospital, Sichuan University, Chengdu, Sichuan 610041, China*

Yueming Song — *Department of Orthopedic Surgery and Orthopedic Research Institue, West China Hospital, Sichuan University, Chengdu, Sichuan 610041, China*

Complete contact information is available at:
https://pubs.acs.org/10.1021/acsomega.0c05191

Author Contributions

‖L.H. and B.C. contributed equally to this work.

Notes

The authors declare no competing financial interest.

ACKNOWLEDGMENTS

REFERENCES

(1) Kaur, M.; Singh, K. Review on titanium and titanium based alloys as biomaterials for orthopaedic applications. *Mater. Sci. Eng. C* **2019**, *102*, 844−862.

(2) Runa, M. J.; Mathew, M. T.; Fernandes, M. H.; Rocha, L. A. First insight on the impact of an osteoblastic layer on the bio-tribocorrosion performance of Ti6Al4V hip implants. *Acta Biomater.* **2015**, *12*, 341−351.

(3) Bosshardt, D. D.; Chappuis, V.; Buser, D. Osseointegration of titanium, titanium alloy and zirconia dental implants: current knowledge and open questions. *Periodontology 2000* **2017**, *73*, 22−40.

(4) Cai, B.; Tan, P.; Jiang, N.; Guo, Z.; Ay, B.; Li, S.; Hou, Y.; Li, Y.; You, Y.; Zhang, L.; Zhu, S. Bioinspired Fabrication of Calcium-Doped TiP Coating with Nanofibrous Microstructure to Accelerate Osseointegration. *Bioconjugate Chem.* **2020**, *31*, 1641−1650.

(5) Facca, S.; Lahiri, D.; Fioretti, F.; Messadeq, N.; Mainard, D.; Benkirane-Jessel, N.; Agarwal, A. In vivo osseointegration of nano-designed composite coatings on titanium implants. *ACS Nano* **2011**, *5*, 4790−4799.

(6) Xiu, P.; Jia, Z.; Lv, J.; Yin, C.; Cheng, Y.; Zhang, K.; Song, C.; Leng, H.; Zheng, Y.; Cai, H.; Liu, Z. Tailored Surface Treatment of 3D Printed Porous Ti6Al4V by Microarc Oxidation for Enhanced Osseointegration via Optimized Bone In-Growth Patterns and Interlocked Bone/Implant Interface. *ACS Appl. Mater. Interfaces* **2016**, *8*, 17964−17975.

(7) Barui, S.; Panda, A. K.; Naskar, S.; Kuppuraj, R.; Basu, S.; Basu, B. 3D inkjet printing of biomaterials with strength reliability and cytocompatibility: Quantitative process strategy for Ti-6Al-4V. *Biomaterials* **2019**, *213*, No. 119212.

(8) Greer, A. I. M.; Goriainov, V.; Kanczler, J.; Black, C. R. M.; Turner, L. A.; Meek, R. M. D.; Burgess, K.; MacLaren, I.; Dalby, M. J.; Oreffo, R. O. C.; Gadegaard, N. Nanopatterned Titanium Implants Accelerate Bone Formation In Vivo. *ACS Appl. Mater. Interfaces* **2020**, *12*, 33541−33549.

(9) Zhao, Q. M.; Sun, Y. Y.; Wu, C. S.; Yang, J.; Bao, G. F.; Cui, Z. M. Enhanced osteogenic activity and antibacterial ability of manganese-titanium dioxide microporous coating on titanium surfaces. *Nanotoxicology* **2020**, *14*, 289−309.

(10) Reznikov, N.; Shahar, R.; Weiner, S. Bone hierarchical structure in three dimensions. *Acta Biomater.* **2014**, *10*, 3815−3826.

(11) Gittens, R. A.; McLachlan, T.; Olivares-Navarrete, R.; Cai, Y.; Berner, S.; Tannenbaum, R.; Schwartz, Z.; Sandhage, K. H.; Boyan, B. D. The effects of combined micron-/submicron-scale surface roughness and nanoscale features on cell proliferation and differentiation. *Biomaterials* **2011**, *32*, 3395−3403.

(12) Cheng, M.; Qiao, Y.; Wang, Q.; Jin, G.; Qin, H.; Zhao, Y.; Peng, X.; Zhang, X.; Liu, X. Calcium Plasma Implanted Titanium Surface with Hierarchical Microstructure for Improving the Bone Formation. *ACS Appl. Mater. Interfaces* **2015**, *7*, 13053−13061.

(13) Mendonça, G.; Mendonça, D. B. S.; Aragão, F. J.; Cooper, L. F. Advancing dental implant surface technology–from micron- to nanotopography. *Biomaterials* **2008**, *29*, 3822−3835.

(14) Huang, Q.; Elkhooly, T. A.; Liu, X.; Zhang, R.; Yang, X.; Shen, Z.; Feng, Q. Effects of hierarchical micro/nano-topographies on the morphology, proliferation and differentiation of osteoblast-like cells. *Colloids Surf., B* **2016**, *145*, 37−45.

(15) Hu, Z.; Wang, X.; Xia, W.; Wang, Z.; Zhang, P.; Xia, L.; Lin, K.; Zhu, M. Nano-Structure Designing Promotion Osseointegration of Hydroxyapatite Coated Ti-6Al-4V Alloy Implants in Diabetic Model. *J. Biomed. Nanotechnol.* **2019**, *15*, 1701−1713.

(16) Gildenhaar, R.; Knabe, C.; Gomes, C.; Linow, U.; Houshmand, A.; Berger, G. Calcium Alkaline Phosphate Scaffolds for Bone Regeneration 3D-Fabricated by Additive Manufacturing. *Key Eng. Mater.* **2011**, *493−494*, 849−854.

(17) Park, J.-W.; Jang, J. H.; Lee, C. S.; Hanawa, T. Osteoconductivity of hydrophilic microstructured titanium implants with phosphate ion chemistry. *Acta Biomater.* **2009**, *5*, 2311−2321.

(18) Chesnutt, B. M.; Viano, A. M.; Yuan, Y.; Yang, Y.; Guda, T.; Appleford, M. R.; Ong, J. L.; Haggard, W. O.; Bumgardner, J. D. Design and characterization of a novel chitosan/nanocrystalline calcium phosphate composite scaffold for bone regeneration. *J. Biomed. Mater. Res., Part A* **2009**, *88A*, 491−502.

(19) Ong, J. L.; Bessho, K.; Cavin, R.; Carnes, D. L. Bone response to radio frequency sputtered calcium phosphate implants and titanium implants in vivo. *J. Biomed. Mater. Res.* **2002**, *59*, 184−190.

(20) Amin Yavari, S.; van der Stok, J.; Chai, Y. C.; Wauthle, R.; Tahmasebi Birgani, Z.; Habibovic, P.; Mulier, M.; Schrooten, J.; Weinans, H.; Zadpoor, A. A. Bone regeneration performance of surface-treated porous titanium. *Biomaterials* **2014**, *35*, 6172−6181.

(21) Li, Y.; Yang, W.; Li, X.; Zhang, X.; Wang, C.; Meng, X.; Pei, Y.; Fan, X.; Lan, P.; Wang, C.; Li, X.; Guo, Z. Improving osteointegration and osteogenesis of three-dimensional porous Ti6Al4V scaffolds by polydopamine-assisted biomimetic hydroxyapatite coating. *ACS Appl. Mater. Interfaces* **2015**, *7*, 5715−5724.

(22) Ma, X. Y.; Feng, Y. F.; Ma, Z. S.; Li, X.; Wang, J.; Wang, L.; Lei, W. The promotion of osteointegration under diabetic conditions using chitosan/hydroxyapatite composite coating on porous titanium surfaces. *Biomaterials* **2014**, *35*, 7259−7270.

(23) Zhang, W.; Cao, H.; Zhang, X.; Li, G.; Chang, Q.; Zhao, J.; Qiao, Y.; Ding, X.; Yang, G.; Liu, X.; Jiang, X. A strontium-incorporated nanoporous titanium implant surface for rapid osseointegration. *Nanoscale* **2016**, *8*, 5291−5301.

(24) Zhang, X.; Lv, Y.; Fu, S.; Wu, Y.; Lu, X.; Yang, L.; Liu, H.; Dong, Z. Synthesis, microstructure, anti-corrosion property and biological performances of Mn-incorporated Ca-P/TiO(2) composite coating fabricated via micro-arc oxidation. *Mater. Sci. Eng. C* **2020**, *117*, No. 111321.

(25) Jayaram, D. T.; Payne, C. K. Intracellular Generation of Superoxide by TiO(2) Nanoparticles Decreases Histone Deacetylase 9 (HDAC9), an Epigenetic Modifier. *Bioconjugate Chem.* **2020**, *31*, 1354−1361.

(26) Clauder, F.; Czerniak, A. S.; Friebe, S.; Mayr, S. G.; Scheinert, D.; Beck-Sickinger, A. G. Endothelialization of Titanium Surfaces by Bioinspired Cell Adhesion Peptide Coatings. *Bioconjugate Chem.* **2019**, *30*, 2664−2674.

(27) Campbell, A. A.; Song, L.; Li, X. S.; Nelson, B. J.; Bottoni, C.; Brooks, D. E.; DeJong, E. S. Development, characterization, and anti-microbial efficacy of hydroxyapatite-chlorhexidine coatings produced by surface-induced mineralization. *J. Biomed. Mater. Res.* **2000**, *53*, 400−407.

(28) Hou, Y.; Yu, L.; Xie, W.; Camacho, L. C.; Zhang, M.; Chu, Z.; Wei, Q.; Haag, R. Correction to Surface Roughness and Substrate Stiffness Synergize To Drive Cellular Mechanoresponse. *Nano Lett.* **2020**, *20*, 4059.

(29) Hou, Y.; Xie, W.; Yu, L.; Camacho, L. C.; Nie, C.; Zhang, M.; Haag, R.; Wei, Q. Surface Roughness Gradients Reveal Topography-Specific Mechanosensitive Responses in Human Mesenchymal Stem Cells. *Small* **2020**, *16*, No. 1905422.

(30) Schüpbach, P.; Glauser, R.; Rocci, A.; Martignoni, M.; Sennerby, L.; Lundgren, A.; Gottlow, J. The human bone-oxidized titanium implant interface: A light microscopic, scanning electron microscopic, back-scatter scanning electron microscopic, and energy-dispersive x-ray study of clinically retrieved dental implants. *Clin. Implant Dent. Relat. Res.* **2005**, *7*, S36−S43.

(31) Ahmad, T.; Byun, H.; Lee, J.; Madhurakat Perikamana, S. K.; Shin, Y. M.; Kim, E. M.; Shin, H. Stem cell spheroids incorporating fibers coated with adenosine and polydopamine as a modular building blocks for bone tissue engineering. *Biomaterials* **2020**, *230*, No. 119652.

(32) Shi, M.; Xia, L.; Chen, Z.; Lv, F.; Zhu, H.; Wei, F.; Han, S.; Chang, J.; Xiao, Y.; Wu, C. Europium-doped mesoporous silica nanosphere as an immune-modulating osteogenesis/angiogenesis agent. *Biomaterials* **2017**, *144*, 176−187.

(33) Wieding, J.; Lindner, T.; Bergschmidt, P.; Bader, R. Biomechanical stability of novel mechanically adapted open-porous titanium scaffolds in metatarsal bone defects of sheep. *Biomaterials* **2015**, *46*, 35−47.

(34) Li, F.; Li, J.; Xu, G.; Liu, G.; Kou, H.; Zhou, L. Fabrication, pore structure and compressive behavior of anisotropic porous titanium for human trabecular bone implant applications. *J. Mech. Behav. Biomed. Mater.* **2015**, *46*, 104−114.

(35) Parthasarathy, J.; Starly, B.; Raman, S.; Christensen, A. Mechanical evaluation of porous titanium (Ti6Al4V) structures with electron beam melting (EBM). *J. Mech. Behav. Biomed. Mater.* **2010**, *3*, 249−259.

(36) Zhang, R.; Elkhooly, T. A.; Huang, Q.; Liu, X.; Yang, X.; Yan, H.; Xiong, Z.; Ma, J.; Feng, Q.; Shen, Z. A dual-layer macro/mesoporous structured TiO(2) surface improves the initial adhesion of osteoblast-like cells. *Mater. Sci. Eng C* **2017**, *78*, 443−451.

(37) Davies, J. E. Bone bonding at natural and biomaterial surfaces. *Biomaterials* **2007**, *28*, 5058−5067.

(38) Davies, J. E.; Ajami, E.; Moineddin, R.; Mendes, V. C. The roles of different scale ranges of surface implant topography on the stability of the bone/implant interface. *Biomaterials* **2013**, *34*, 3535−3546.

(39) Davies, J. E.; Mendes, V. C.; Ko, J. C.; Ajami, E. Topographic scale-range synergy at the functional bone/implant interface. *Biomaterials* **2014**, *35*, 25−35.

(40) Chen, Y.; Feng, B.; Zhu, Y.; Weng, J.; Wang, J.; Lu, X. Preparation and characterization of a novel porous titanium scaffold with 3D hierarchical porous structures. *J. Mater. Sci.: Mater. Med.* **2011**, *22*, 839−844.

(41) Jonitz-Heincke, A.; Wieding, J.; Schulze, C.; Hansmann, D.; Bader, R. Comparative Analysis of the Oxygen Supply and Viability of Human Osteoblasts in Three-Dimensional Titanium Scaffolds Produced by Laser-Beam or Electron-Beam Melting. *Materials* **2013**, *6*, 5398−5409.